Retrieval of Optical Depth for Heavy Smoke Aerosol Plumes: Uncertainties and Sensitivities to the Optical Properties

JEFF WONG AND ZHANQING LI*

Canada Centre for Remote Sensing, Ottawa, Ontario, Canada

ABSTRACT

This paper is concerned with uncertainties in the Advanced Very High Resolution Radiometer (AVHRR)-based retrieval of optical depth for heavy smoke aerosol plumes generated from forest fires that occurred in Canada due to a lack of knowledge on their optical properties (single-scattering albedo and asymmetry parameter). Typical values of the optical properties for smoke aerosols derived from such field experiments as Smoke, Clouds, and Radiation-Brazil (SCAR-B); Transport and Atmospheric Chemistry near the Equator-Atlantic (TRACE-A); Biomass Burning Airborne and Spaceborne Experiment in the Amazonas (BASE-A); and Boreal Ecosystem–Atmosphere Study (BOREAS) were first assumed for retrieving smoke optical depths. It is found that the maximum top-of-atmosphere (TOA) reflectance values calculated by models with these aerosol parameters are less than observations whose values are considerably higher. A successful retrieval would require an aerosol model that either has a substantially smaller asymmetry parameter ($g < 0.4$ versus $g > 0.5$), or higher single-scattering albedo ($\omega \gg 0.9$ versus $\omega < 0.9$), or both (e.g., $g = 0.39$ and $\omega = 0.91$ versus $g = 0.57$ and $\omega = 0.87$) than the existing models. Several potential causes were examined including small smoke particle size, low black carbon content, humidity effect, calibration errors, inaccurate surface albedo, mixture of cloud and aerosol layers, etc. A more sound smoke aerosol model is proposed that has a lower content of black carbon (mass ratio $= 0.015$) and smaller size (mean radius $= 0.02$ μm for dry smoke particles), together with consideration of the effect of relative humidity. Ground-based observations of smoke suggest that for $\tau < 2.5$ there is an increasing trend in ω and a decreasing trend in g with increases in τ, which is consistent with the results of satellite retrievals. Using these relationships as constraints, more plausible values of τ can be obtained for heavy smoke aerosol. The possibility of smoke–cloud mixtures is also considered, which can also lead to high TOA reflectances. However, without measurements, the hypothesis can be neither accepted nor negated. The study demonstrates that without independent assessments of the optical properties, large uncertainties would be incurred in the retrieved values of optical depth for heavy smoke aerosol plumes.

1. Introduction

Every year, a large number of fires occur during the summer months across the boreal forest zone located in northern latitudes (Stocks 1991; Li et al. 2000). These fires release smoke aerosol particles along with carbon monoxide, carbon dioxide, and other trace gases (Kaufman et al. 1994). These emissions have significant impacts on both short-term weather conditions (cooling due to aerosol particles) and long-term climate changes (warming due to trace gases). Information on the optical properties of smoke aerosol is crucial to the understanding of its influence on the earth's climate system. It is

worth noting that the radiative forcing of all aerosols is comparable to the radiative forcing due to the increases in greenhouse gas concentrations in the atmosphere since the beginning of the industrial age, which is estimated to be $+2.45$ W m^{-2} (Schimel et al. 1996). Note that there is a very large uncertainty (a factor of 3) in the estimate of radiative forcing due to smoke aerosols. The large uncertainty is attributed primarily to the poor knowledge of their loading and optical properties.

Aerosol optical depth τ has been derived both from in situ and remote sensing measurements. Satellite remote sensing has a major advantage of being able to cover large spatial areas routinely, but it suffers from some inherent limitations. Smoke aerosols are usually located over land areas near the sources of combustion. The reflectance of land surfaces is usually more variable and larger in magnitude than the reflectance of water bodies. The signal observed by satellites is the convolution of signals due to aerosol and the underlying surface. These contributions are difficult to separate because τ is usually small. As a result, the retrieval of τ

* Current affiliation: Earth System Science Interdisciplinary Center, Department of Meteorology, University of Maryland, College Park, Maryland.

Corresponding author address: Zhanqing Li, Dept. of Meteorology, University of Maryland, 2335 Computes and Space Sciences Building, College Park, MD 20742-2425.
E-mail: zli@atmos.umd.edu

has been performed primarily over oceans (Mishchenko et al. 1999; Stowe et al. 1997; Higurashi and Nakajima 1999). A few attempts were made over small areas of land where the surface reflectance characteristics are well known and relatively uniform in order to minimize the error in the retrievals (Holben et al. 1992). The retrieval over land is more feasible for heavy loading events such as smoke that shows a large contrast against the environment. For example, Kaufman et al. (1990) and Ferrare et al. (1990) used the contrast in observations between smoky and smoke-free regions in the study area to help isolate the aerosol effect. Retrieval of τ is usually based on the comparison of observed visible top-of-atmosphere (TOA) reflectances with model calculations (Soufflet et al. 1997; Liousse et al. 1997; Molineaux et al. 1998).

Using satellite observations at one wavelength, it may be possible to determine one aerosol property, such as the optical depth (King et al. 1999), while other properties, such as the single-scattering albedo and the asymmetry parameter are assumed based on other independent information, such as in situ measurements. Our understanding of smoke aerosols has improved considerably thanks to the many field campaigns such as the Smoke, Clouds, and Radiation-Brazil (SCAR-B; Kaufman et al. 1998), the Amazon Boundary Layer Experiment (ABLE-2A; Harriss et al. 1988), the Biomass Burning Airborne and Spaceborne Experiment in the Amazonas (BASE-A; Kaufman et al. 1992), the Transport and Atmospheric Chemistry near the Equator-Atlantic (TRACE-A; Fishman et al. 1992), and the Boreal Ecosystem–Atmosphere Study (BOREAS) projects (Sellers et al. 1997). Retrieved single scattering albedos have been reported as low as 0.6 (Miller and O'Neill 1997) and as high as 1.0 (Ferrare et al. 1990). Since the optical properties of smoke depend on many factors such as the burning material and burning conditions, it is not surprising that single scattering albedos vary over such a large range.

In contrast to the numerous experiments addressing smoke aerosol from tropical fires, few field campaigns were devoted to smoke generated from boreal forest fires. This study reveals large uncertainties in the retrieval of aerosol optical depth for smoke generated from forest fires in the boreal forests of Canada resulting from a poor knowledge of the characteristics of the smoke. The study employs observations from the Advanced Very High Resolution Radiometer (AVHRR), together with some ground-based observations. Aerosol properties obtained from the aforementioned field campaigns are used. In order to minimize the impact of surface reflectance and to better isolate the problem, only heavy smoke plumes are considered, with reflectances exceeding 0.30, which can lead to retrieved optical depths in excess of 2.0 depending on the aerosol model. The retrieval will be shown to be very sensitive to the assumptions made regarding smoke aerosol optical properties. It will be demonstrated that the optical

depth cannot be retrieved with conventional values of the single scattering albedo ω and the asymmetry parameter g. The properties obtained from fire experiments that took place in tropical regions do not seem to apply to heavy smoke plumes generated by boreal forest fires in Canada.

The effect of relative humidity on the smoke aerosol is considered, which was not considered carefully in previous studies of smoke (Ferrare et al. 1990; Kaufman et al. 1992). This is partly due to the limited understanding of the hygroscopic nature of carbonaceous aerosols. The effect of relative humidity on the light-scattering properties of biomass burning aerosols was measured during SCAR-B (Kotchenruther and Hobbs 1998). Using these measurements, the optical properties of smoke aerosol are calculated as functions of relative humidity. With these optical properties, the retrieval of optical depth is attempted assuming different values for the relative humidity in the smoke plumes. The results indicate that hygroscopic growth needs to be considered in the retrieval procedure.

Finally, as an alternative approach to the problem, relationships between smoke aerosol optical properties are examined using both satellite and ground-based observations. From the data, relationships are examined and parameterized between ω and τ and between g and τ. The parameterizations are then employed in the retrieval of smoke aerosol optical depth. It will be shown that use of these parameterizations can lead to more meaningful retrievals of τ. On the other hand, since the parameterizations are based on data with optical depths less than 2.5, the accuracy of the retrieved optical depths is yet to be validated with independent observations for higher optical depths.

2. Retrieval of optical depth

a. Retrieval technique

This study employs the TOA reflectance observed by channel 1 of the AVHRR on board the National Oceanic and Atmospheric Administration (NOAA) satellite. The spectral response function for the *NOAA-14* AVHRR (Kidwell 1991) is used to simulate satellite measurements at channel 1 centered around 0.65 μm (R^{TOA}). In order to estimate τ, R^{TOA} is compared to precalculated lookup tables (LUTs) of reflectance ρ^{TOA}. The discrete-ordinate radiative transfer program (Stamnes et al. 1988) is used to calculate the LUT corresponding to a particular solar zenith angle θ_0, satellite zenith angle θ_v, relative azimuth angle $\Delta\phi$, surface albedo A_s, and smoke aerosol optical depth τ for a given set of aerosol optical properties as discussed below. The smoke aerosol is confined to the bottom 4 km of the column (Anderson et al. 1996). The optical properties of the atmosphere are calculated with the Moderate-Resolution Atmospheric Radiance and Transmittance Model 3.5 code (Berk et al. 1989) assuming the standard midlatitude

summer atmospheric profile (WMO 1986). Note that the profiles of atmospheric constituents have only minor effects on the calculated reflectance in channel 1 of the AVHRR. Rayleigh scattering and surface reflection are the driving factors for the variation of ρ^{TOA} under smoke-free conditions. A land surface albedo product is used that was retrieved from smoke-free AVHRR reflectance data for each 1-km pixel and corrected for the atmospheric effect and the dependence on viewing geometry (Li et al. 1996; Cihlar et al. 1997a). This annual surface reflectance product is normalized to the nadir view and 45° solar zenith angle within each 10-day period. Using this dataset together with the bidirectional reflectance distribution function (Li et al. 1996) for each of the 14 surface types classified in the data product, surface reflectance at any particular viewing geometry can be estimated. Since the satellite-observed reflectance is due to the aerosol and surface combined, their respective contributions to the total reflectance must be separated. Accuracy in the retrieved optical depth depends partially on the accuracy of the estimated surface reflectance, in particular for cases of low aerosol loading.

The extinction coefficient k_{ext}, single scattering albedo ω, and scattering phase function P of smoke aerosol are calculated using Mie theory. A single accumulation mode with a lognormal function is assumed for the aerosol size distribution dN/dr. The accumulation mode dominates radiative processes (Miller and O'Neill 1997; Remer et al. 1998). Distributions of multiple modes can be simulated with an appropriate single mode (Kaufman et al. 1997). A geometric mean radius of $r_g = 0.05$ μm and a standard deviation of $\ln\sigma_g = 0.6$ were selected initially, which are representative of the smoke aerosol accumulation mode (Remer et al. 1998; Ross et al. 1998) observed during the SCAR-B experiment. This value of r_g is comparable to the average size distribution obtained during ABLE-2A (Andreae et al. 1988). A value of 1.56 is used for the real part of the refractive index of smoke m_r obtained by Yamasoe et al. (1998) in SCAR-B. The imaginary part m_i is assumed to be 0.025 so that the single-scattering albedo for this aerosol model is $\omega = 0.86$, an average value retrieved for biomass burning aerosols observed during SCAR-B (Dubovik et al. 1998; Kaufman et al. 1998). The asymmetry parameter for this aerosol model is $g = 0.57$, which is comparable to the value of 0.58 retrieved by Holben et al. (1996) for biomass burning aerosols.

b. Sensitivity to smoke aerosol properties

Identification of smoke aerosol from AVHRR imagery was done by an artificial neural network (Li et al. 2001). The neural network approach has the capability of "learning" from training datasets, and handling complex relationships between various channels in linear or nonlinear form. More importantly, it generates quantitative and continuous indices of smoke, as well as other subjects. The smoke index provides a measure of both

the concentration of smoke and the mixing among scene types (i.e., smoke–cloud, smoke–land, smoke–land–cloud). This study is concentrated on heavy smoke plumes with high smoke concentration. Figure 1a is an AVHRR image showing smoky pixels separated from cloudy and cloud- and aerosol-free pixels classified using the neural network technique. The scene is located in Manitoba, Canada, on 6 August 1998, while many other scenes containing heavy smoke were also investigated with similar findings. Figure 1b shows a grayscale image of the retrieved τ. Figure 2 shows the histogram of the retrieved τ corresponding to this panel. A significant number of pixels have τ exceeding 2.0. In Fig. 1b, there are holes in the heart of smoke plumes where the inversion algorithm failed to retrieve valid values of τ because the observed reflectance exceeds the maximum value computed by the radiative transfer model. Higher reflectance values can result from single scattering albedos ω larger than the value of 0.87 as assumed for the current smoke aerosol model, or from asymmetry g smaller than the value of 0.57 being used, or both. Higher ω can be obtained by decreasing the imaginary part of the refractive index or the black carbon content of the particles. If the retrieval is attempted using an aerosol model with $m_i = 0.015$ (which increases ω to 0.91), the holes shrink as shown in Fig. 1c. If m_i is reduced to 0.005 ($\omega = 0.97$), most of the holes in the τ image are filled, as shown in Fig. 1d. Further reduction in m_i continues to fill in the remaining holes. These decreases in m_i do not significantly alter the calculated value of g. This problem in the retrieval of smoke aerosol optical depth is not an isolated incident. It happens for the majority of thick smoke plumes on other days and in other regions. An alternative method of improving the retrieval of τ is to decrease g. Figures 1e and 1f shows the image of retrieved τ as g decreases to 0.40 and 0.22, while ω is kept fixed at 0.87.

The sensitivity of retrieving τ to the value of ω is shown in Fig. 3, which plots ρ^{TOA} as a function of τ for various magnitudes of ω ranging from 0.86 to 0.98, under a viewing geometry given by $(\theta_0, \theta_v, \Delta\phi) = (43°, 13°, 30°)$, and an underlying surface albedo of 0.05. A smoke aerosol model with $r_g = 0.05$ μm is considered. It is seen that ρ^{TOA} saturates at a level that depends strongly on the value of ω. For a particular R^{TOA}, it is impossible to find a matching ρ^{TOA} to obtain an estimate of τ if ω is too low. The saturation level can also be raised by a reduction in g. A low asymmetry parameter is an indication of small particle size. Uncertainties in the size distribution can lead to significant differences in the radiative transfer (Chylek and Wong 1995). The smoke shown in Fig. 1 is fresh, which may contain smaller particles than older mixed smoke (Kaufman et al. 1994). To examine this possibility, another aerosol model is considered with $r_g = 0.03$ μm and $m_i = 0.015$ so that $\omega = 0.86$ and g is reduced from 0.57 to 0.40. Though ρ^{TOA} values are higher (as shown in Fig. 3), they are not increased enough to fill in the holes in the image
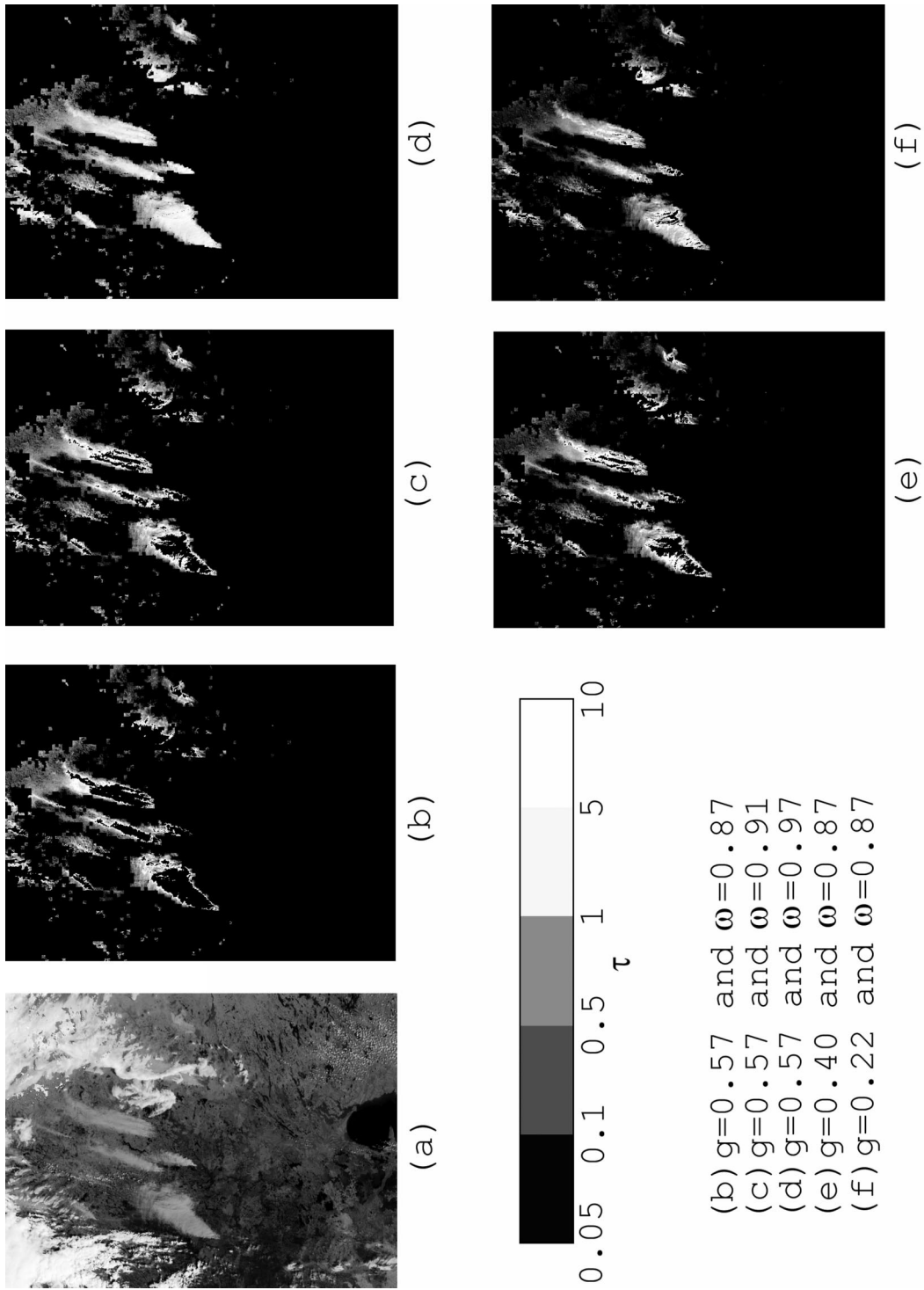
FIG. 1. (a) AVHRR image (visible channel) on 6 Aug 1998 with smoke pixels (gray plumes) separated from cloudy (white) and clear pixels (darker background). (b)–(d) Images showing retrieved smoke aerosol optical depth τ assuming three different values of single scattering albedo ($\omega = 0.86$, 0.91, and 0.97) and a fixed asymmetry parameter ($g = 0.57$). (e), (f) Retrieved τ for fixed ω (0.86) and variable g (0.40 and 0.22).
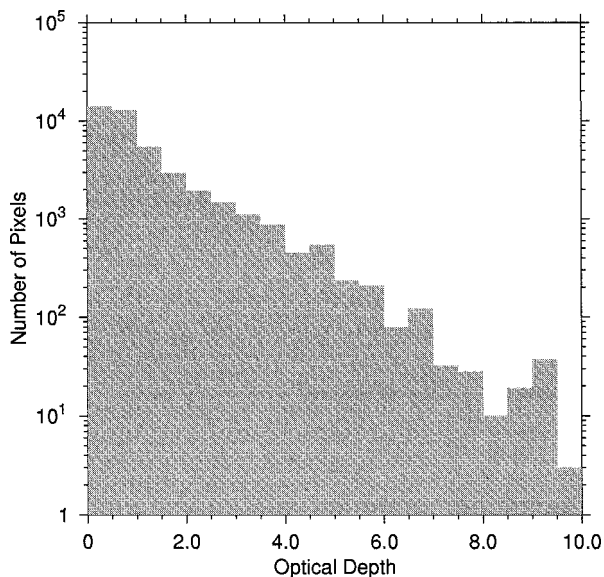
FIG. 2. Histogram showing the distribution of retrieved smoke aerosol optical depth when the smoke aerosol is modeled with $g = 0.57$ and $\omega = 0.86$.

FIG. 3. Model-calculated TOA reflectance as a function of τ for an aerosol model with fixed r_g (0.05 μm) and variable ω (0.86, 0.91, 0.96, and 0.98), in comparison with the curve (squares) corresponding to a different value of r_g (0.03 μm) and ω (0.86). The viewing geometry is given by $\theta_0 = 43°$, $\theta_v = 13°$, $\Delta\phi = 30°$ and the surface albedo is 0.05.

of τ (as shown in Fig. 1e). An increase in ω is more effective than a decrease in g for retrieving meaningful values of τ.

A lower ω can result from a lower content of the black carbon in the smoke aerosol. Hobbs et al. (1996) measured the ratio of black carbon to total carbon mass in smoke χ for prescribed burns in Oregon and Washington during the Smoke, Clouds, and Radiation–California experiment. They obtained values between 0.052 and 0.077. Values between 0.05 and 0.15 were observed by Martins et al. (1996). Measurements from prescribed burns in Ontario, Canada, have χ values between 0.011 and 0.092 (Mazurek et al. 1991). Assuming a lognormal size distribution characterized by $r_g = 0.05$ μm, this range of observed χ corresponds to values of ω ranging from 0.75 to 0.97. During BASE-A, the values of ω obtained ranged from 0.89 to 0.91 (Kaufman et al. 1992). Anderson et al. (1996) obtained values ranging from 0.79 to 0.82 during the TRACE-A experiment. These estimates do not differ significantly from those derived from dispersed smoke aerosol originating from boreal fires. BOREAS took place in the provinces of Manitoba and Saskatchewan, Canada, in 1994–95. Using BOREAS data, Li and Kou (1998) inferred the single-scattering albedo by combining TOA visible reflectance from Geostationary Operational Environmental Satellite (GOES) measurements with ground-based observations of τ from the Aerosol Robotic Network (AERONET; Holben et al. 1998). The frequency distribution of inferred ω, shown in Fig. 4, suggests that the average value of ω is 0.87. The almucantar measurements of the AERONET dataset alone can also be used to retrieve the single, scattering albedo (Dubovik et al. 1998). The values obtained from BOREAS are
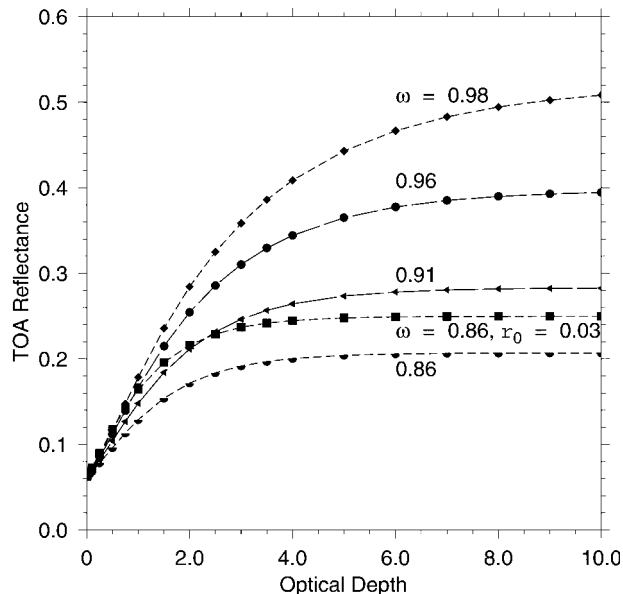
quite variable, but the arithmetic mean value is also 0.87 (Markham et al. 1997). Miller and O'Neill (1997) made aircraft observations of smoke aerosols near the BOREAS sites and found that $\omega = 0.60$ for the observed low-altitude smoke layer and $\omega = 0.90$ for a higher-altitude smoke layer. In contrast, Ferrare et al. (1990) retrieved higher values of ω between 0.90 and 1.0 for smoke aerosols that originated from forest fires in Canada. Note that all these estimates are for relatively thin smoke (with τ typically less than 1 $\sim$ 2), since heavy smoke near the source of burning was not observed, or may have been screened out together with clouds. High values of ω have been obtained before (Ferrare et al. 1990), and it is possible that heavy smoke plumes tend to have higher values of ω.

Uncertainty in the retrieved τ could arise from errors associated with estimates of surface albedo for the underlying land surfaces. To examine such an effect, the retrieval was performed with the estimated surface albedo being multiplied by a factor of 1.1. The relative difference is within 10% for $\tau > 0.5$ but can be much larger than 50% when $\tau < 0.2$. The accuracy of the estimated reflectance is on the order of 20% (Cihlar et al. 1997b). Figure 5 shows the calculated TOA reflectance as a function of smoke aerosol optical depth for two distinct surface reflectance values (0.0 and 0.15). The calculations were done for a particular viewing geometry given by $\theta_0 = 45°$, $\theta_v = 20°$, and $\Delta\phi = 35°$ using a smoke aerosol model with $g = 0.57$ and $\omega = 0.86$. This figure demonstrates that the retrieved aerosol optical depth is sensitive to the surface reflectance only
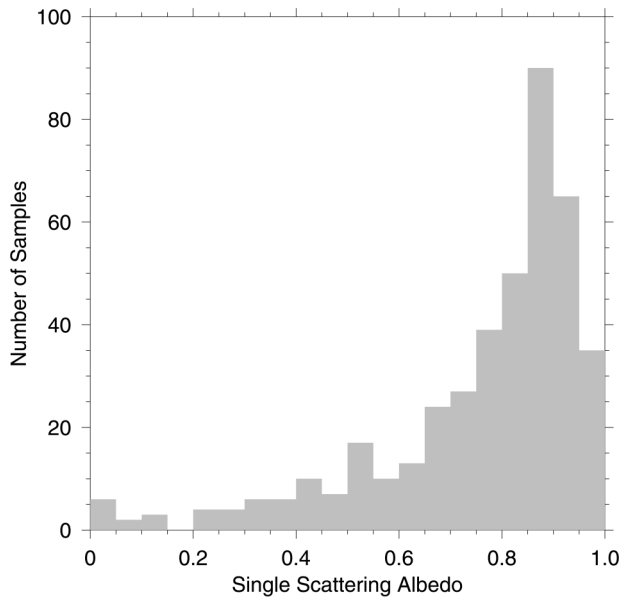
FIG. 4. Frequency distribution of aerosol single scattering albedo ω inferred from the combined datasets of GOES and AERONET obtained during BOREAS following the approach of Li and Kou (1998).
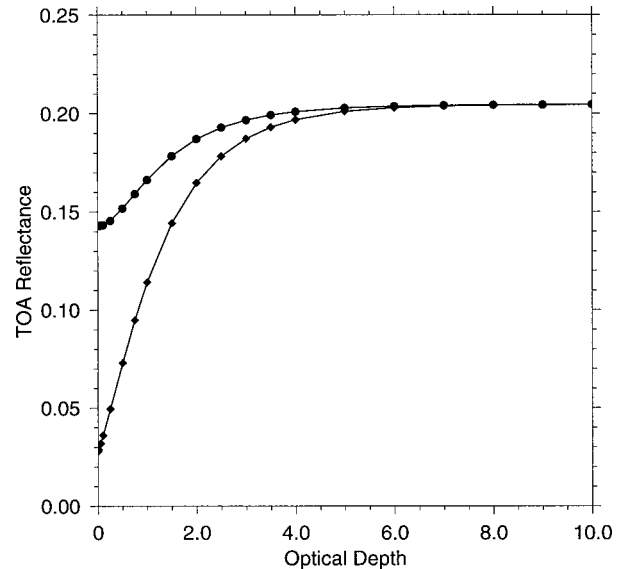

FIG. 5. Calculated TOA reflectance as a function of τ for an aerosol model with $g = 0.57$ and $\omega = 0.86$. The viewing geometry is given by $\theta_0 = 45°$, $\theta_v = 20°$, $\Delta\phi = 35°$. The curve drawn with diamonds corresponds to a surface albedo of 0.0, and the curve drawn with solid circles corresponds to a surface albedo of 0.15.

for low-aerosol loading. For heavy aerosol cases, the maximum TOA reflectance is weakly affected by the surface reflectance. For $\tau > 4$, TOA reflectance is essentially independent of the surface reflectance. Since the current study is concerned with very high aerosol loading, errors in surface albedo are unlikely the cause for the failure of retrieving τ.

Another potential source of uncertainty is the calibration of the AVHRR data. Since AVHRR does not have onboard absolute calibration for its solar channels, postlaunch relative calibration was applied based on the method of Rao and Chen (1996). In addition, there is an independent set of calibration coefficients employed in the International Satellite Cloud Climatology Project (Brest et al. 1997). Use of the latter calibration produces even higher TOA albedos. Relative and absolute uncertainties in the calibration of visible radiance were estimated to be less than 5% and 10%, respectively (Rossow and Schiffer 1999). It is thus unlikely that the higher reflectance from satellite observation is an artifact due to calibration.

c. Effects of relative humidity

Another factor that has not been taken into account carefully in many previous studies is the effect of relative humidity on smoke aerosol, since carbonaceous aerosols are not as hygroscopic as other types of aerosols such as sulfates, nitrates, and sea salt. For a given relative humidity H, the amount of water vapor condensed onto the aerosol particles is contingent upon their chemical composition. Not only does the size of the particle

increase, the effective refractive index of the particle also changes. Observations indicate that the change in the light-scattering coefficient k_{sc} of carbonaceous aerosols with H is much smaller than that of sulfate aerosols (Hobbs et al. 1997; Kotchenruther and Hobbs 1998). But unlike sulfate aerosols, carbonaceous aerosols are absorbing and thus H might have a strong effect on ω.

The smoke aerosol models that are used in satellite remote sensing applications usually assume a fixed amount of water condensation (Ferrare et al. 1990; Kaufman et al. 1992) as an average state, since H within smoke plumes is usually not well known. For example, Kaufman et al. (1994) suggest that at a relative humidity of 0.70, 50% of the particle volume is water. Hobbs et al. (1996) measured an H of 0.85 in the smoke plume, during the ignition phase of a prescribed burn, that decreased to 0.65 when the burn evolved to the flaming phase, while H of the ambient air was only 0.35.

To calculate the optical properties of smoke as functions of H, smoke particles are assumed to be internal mixtures of water, black carbon, and organic matter. A layered-sphere model (Toon and Ackerman 1981) is used with a central black carbon core surrounded by a shell composed of water and organic matter. The mass density of the black carbon core is taken to be 1.8 g cm^{-3} and the density of the organic matter is taken to be 1.2 g cm^{-3} (Ross et al. 1998). Values of 1.75 + i0.44 (d'Almeida et al. 1991) and 1.56 + i0.0035 (Remer et al. 1998; Yamasoe et al. 1998) are used for the refractive indices of the black carbon and organic matter, respectively, and the refractive index of water was reported by Hale and Querry (1973) and Kou et al. (1993). The
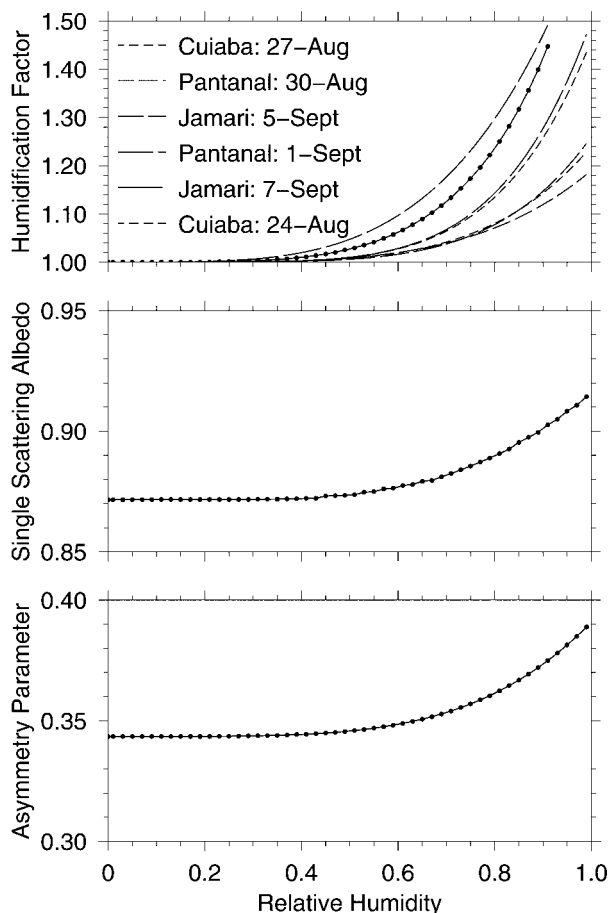
FIG. 6. (top) Model-calculated humidification factor as a function of relative humidity (black dotted line) along with Ross et al.'s (1998) parameterized observations for different days and locations in Brazil (dashed lines). (middle), (bottom) Model-calculated single scattering albedo and asymmetry parameter as a function of relative humidity.

refractive index of the shell is estimated using the Bruggeman effective medium approximation (Chylek et al. 2000). Assuming that the size distribution of the hydrated aerosol is $r_g = 0.05$ μm, the size distribution of the dry smoke aerosol may be characterized by $r_g = 0.02$ μm.

Since the physical and chemical properties of carbonaceous aerosols is not well known, it is not possible to use the Kohler equation (Chylek and Wong 1998; Konopka 1996) to predict the amount of water that condenses on the smoke particles for a given H. Instead, a growth model is assumed such that the change in the scattering coefficient k_{sc} with H is consistent with humidification factors [$F = k_{sc}(H)/k_{sc}(H = 0)$] observed by Hobbs et al. (1997), Kotchenruther and Hobbs (1998), and Ross et al. (1998). The top panel of Fig. 6 shows the calculated F (the dotted black line) along with Ross et al.'s (parameterized) observations for different days and different locations in Brazil (dashed lines). Note that the observations cover a range of H between 0.30 and 0.85. A χ value of 0.015 is considered so that

the calculated ω for the dry particles is approximately 0.86, as shown in the middle panel, which increases to 0.9 when $H = 0.99$. On the other hand, the radiative effect due to the increase in ω is countered by the increase in g shown in the bottom panel. However, the effect on TOA reflectance of the increase in g is not as large as that of the increase in ω, so that modeled TOA albedo keeps increasing to allow for a valid retrieval of τ. Figure 7 shows the image of retrieved τ using this aerosol model. Most of the holes in the smoke plumes are filled as the relative humidity is increased from 0.00 to 0.99. The latter corresponds to $g = 0.39$ and $\omega = 0.91$. Note that the value of ω is not as large as that specified earlier, due to a lower value of g. Though consideration of the hygroscopic growth of smoke particles allows for the retrieval of optical depth, it is difficult to use relative humidity–dependent optical properties in the retrieval algorithm because the relative humidity in smoke plumes is not readily known.

d. Relationships between the optical properties

As an alternative approach to the problem, correlations between observed optical properties are considered. Figure 8 shows the relationship between observed ω and τ. The top panel of Fig. 8 shows the relationship between retrieved ω and τ derived from the BOREAS dataset using Li and Kou (1998)'s method, and the middle panel is derived from the AERONET dataset based on Dubovik et al. (1998)'s work. Note that the AERONET data are for all aerosol and the observed trends are not solely due to smoke aerosol. Though there is a wide range of scatter in the points, there appears to be an increasing trend in ω as τ increases, indicated by the solid curves given by numerical fits of the data points to the following function:

$$\omega = 1 - a/(\tau + b), \qquad (1)$$

where a and b are fitted coefficients. In the top panel, $a = 0.13$ and $b = 0.26$; and in the middle panel, $a = 0.092$ and $b = 0.56$. Calculations based on the Mie theory show that, for particles less than 0.2 μm in radius, ω tends to increase with increasing particle size. Therefore Eq. (1) suggests that particle size grows with increasing optical depth, which is consistent with Remer et al.'s (1998) results. The bottom panel shows a declining trend of g with increasing τ, calculated from the retrieved size distribution and complex refractive index in the AERONET datasets. The solid line in the panel is a linear fit to the data points:

$$g = -0.031 \, \tau + 0.635. \qquad (2)$$

The declining trend in g suggests that particle size decreases as τ increases. This seems to contradict the increasing trend in size suggested by Eq. (1). However, these trends are derived from observations of all aerosol types. The dominant aerosol species may vary with aerosol loading. Therefore, the observed correlations
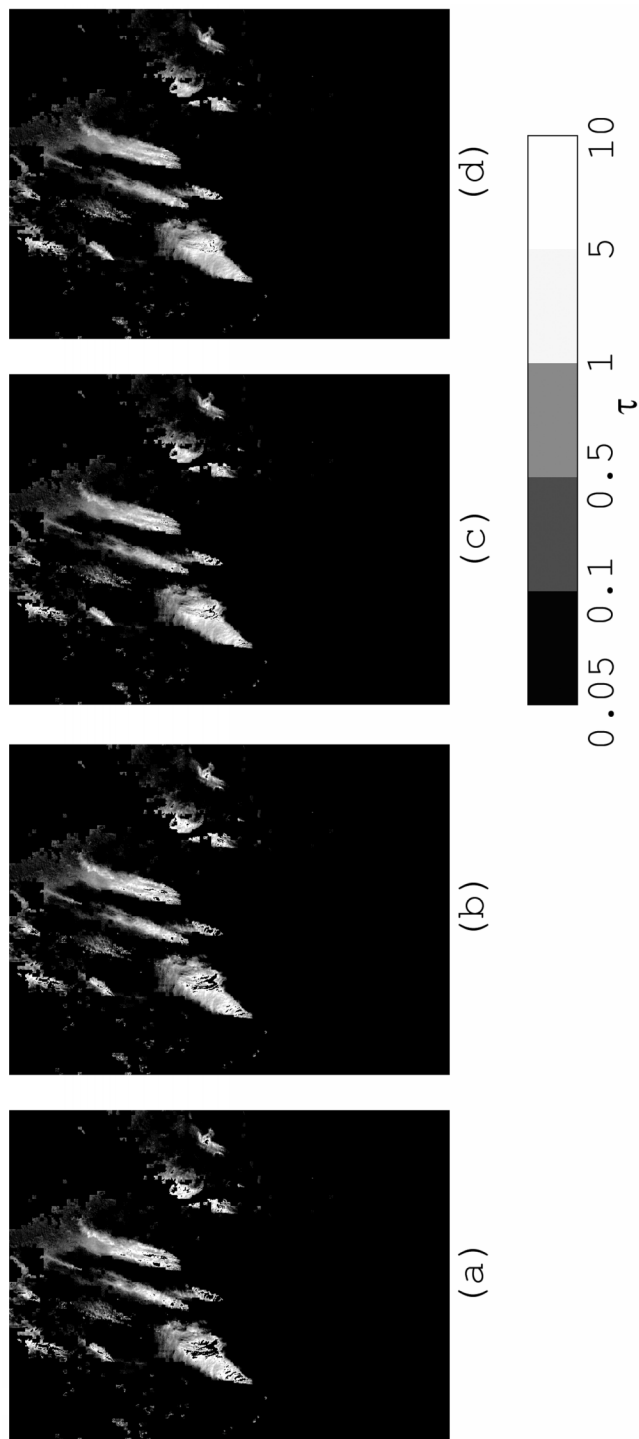
Fig. 7. Images of retrieved τ using a smoke model with $r_g = 0.02$ μm and $\chi = 0.015$ and different values of relative humidity: (a) $H = 0.0$, (b) 0.71, (c) 0.91, and (d) 0.99.
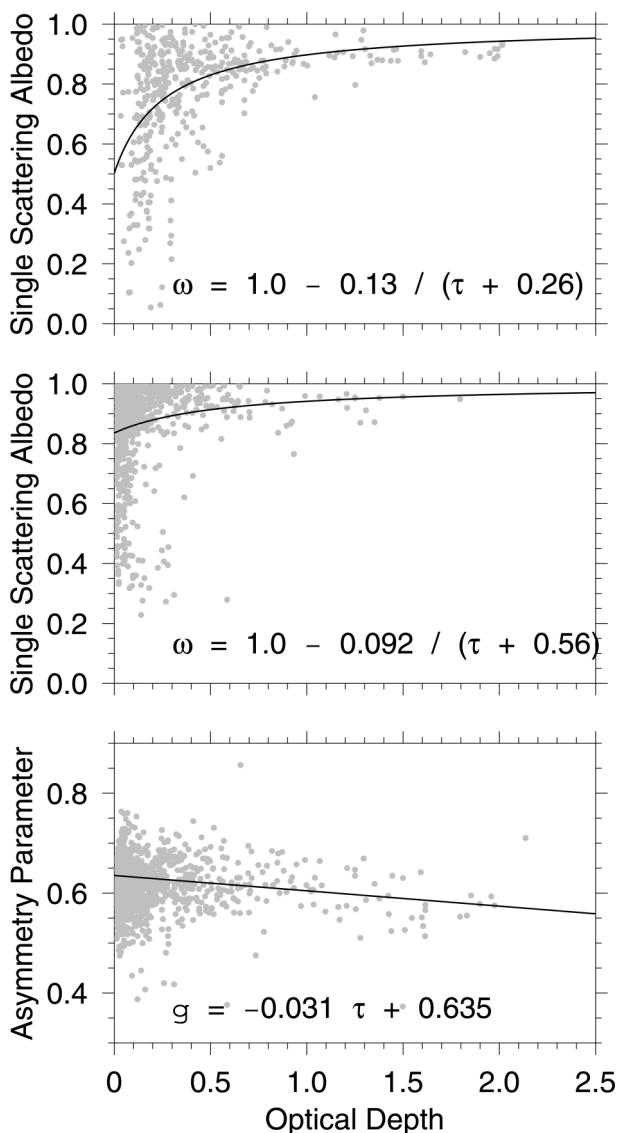
FIG. 8. The relationship between ω and τ for Canadian boreal forest fire smoke obtained following (top) Li and Kou (1998) and (middle) from the AERONET database. (bottom) The relationship between g and τ from AERONET.

FIG. 9. The histograms of the difference (in %) in retrieved τ using a fixed ω with respect to the retrieved τ using a ω–τ constraint. The light gray histogram corresponds to the fixed value of $\omega = 0.97$ and the dark one to $\omega = 0.87$. The histograms are scaled to the total number of smoke pixels.

between optical properties are not due to changes in particle size alone. Particle composition and refractive index also contribute to the trends. For example, the declining trend in g may be due to a decrease in particle size and the increasing trend in ω may be caused primarily by lower imaginary refractive index of the aerosol. The trends in g and ω, described by Eqs. (1) and (2), are qualitatively consistent with our findings, but they are not conclusive since the data are limited to $\tau < 2.5$.

Bearing this limitation in mind, the retrieval algorithm was applied tentatively to the image shown in Fig. 1a using the relationship between ω and τ suggested in the top panel of Fig. 8 as a constraint and with an asym-
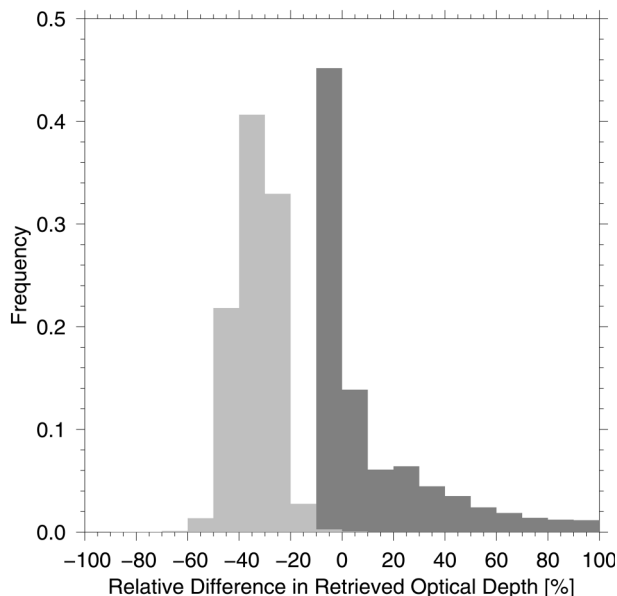
metry parameter fixed at 0.57. Figure 9 shows the histogram of the relative difference (in percent in the retrieved optical depth when using a fixed ω in the retrieval algorithm relative to the optical depth obtained when using the ω–τ constraint. The histogram is scaled to the total number of smoky pixels in the image. The histogram with the light gray bars corresponds to the use of $\omega = 0.97$, and the dark gray bars to $\omega = 0.87$. The retrieved optical depth when using $\omega = 0.97$ is generally lower than the optical depth retrieved using the constraint, while the retrieved optical depth is higher when $\omega = 0.87$ is used. If the ω–τ constraint is valid for $\tau > 2.5$, then the histograms suggest that using a fixed ω throughout the entire smoke plume leads to large errors in retrieved τ. The peak for the $\omega = 0.97$ case is at a relative difference of -35%. The peak for the $\omega = 0.87$ histogram is at -5%, but the distribution is skewed with many points showing a positive relative difference. Figure 10a shows the histogram of the single scattering albedo used in retrieving τ. Only pixels with $\tau > 1.0$ are considered in this histogram. Among the selected smoky pixels, the mode value of ω is around 0.93 with the majority being larger than that.

One may apply both the ω–τ and g–τ constraints in the retrieval. To this end, an initial retrieval of optical depth is performed using an aerosol single scattering albedo of 0.87 and an asymmetry parameter of 0.57. If the retrieval fails, then ω is increased and g is decreased until a valid value of optical depth is obtained. New estimates of ω and g are obtained by using the constraint equations [Eqs. (1) and (2)]. An iterative procedure is
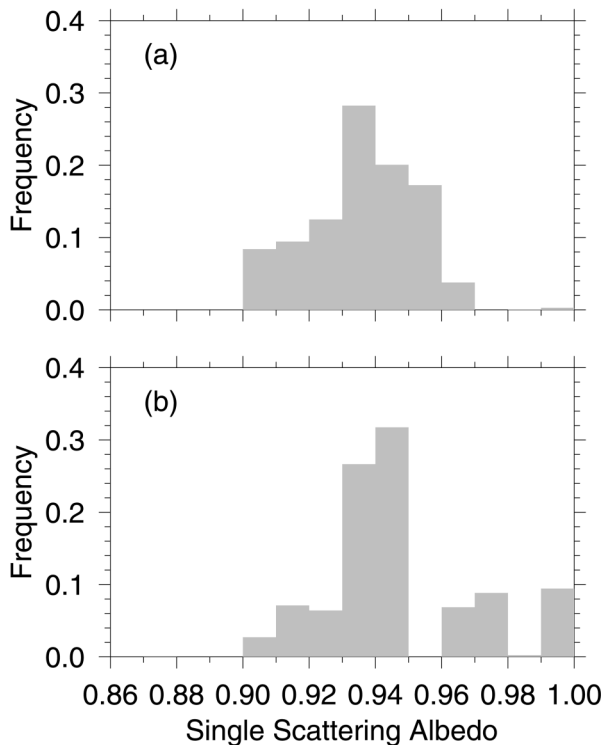
FIG. 11. The histogram of asymmetry parameters retrieved using both $\omega-\tau$ and $g-\tau$ constraints for smoke aerosol optical depth $\tau >$ 1.0.

FIG. 10. The histograms of single scattering albedos retrieved using (a) a $\omega-\tau$ constraint alone, and (b) both $\omega-\tau$ and $g-\tau$ constraints for smoke aerosol optical depth $\tau >$ 1.0.

plume is modeled as a mixture of smoke aerosols with $\omega = 0.86$ and cumulus cloud droplets. The holes in the resulting image of optical depth can be readily filled. Therefore, a smoke–cloud mixture could account for the high TOA reflectance observed. Unfortunately, we cannot validate this hypothesis due to the lack of observations. Without proper observations, it is difficult to choose an appropriate model of the smoke and cloud particle mixture. It is thus recommended for future field campaigns to collect samples of both smoke particles and water droplets, if any, inside smoke plume, especially near fire sites.

begun with the retrieval of a new value of optical depth and subsequent refinement of the optical properties. The iteration is stopped when the values of the optical properties have converged. Figure 10b shows the new histogram of retrieved ω obtained using both constraints on ω and on g. The distribution of ω does not change too much with a peak still around 0.94, but there are more large values. The retrieved g ranges from 0.4 to 0.62, while the majority falls between 0.56 and 0.6, as shown in the histogram of Fig. 11.

These results demonstrate that it is possible to retrieve the optical depth of smoke in heavy smoke plumes if constraints are applied between the aerosol optical properties. However, these results depend on the validity of the $\omega-\tau$ and $g-\tau$ relationships.

e. Smoke and cloud mixture

Other plausible scenarios that might explain the observed higher values of reflectance include the possibility of a thin layer of clouds situated above a smoke plume, or that the smoke plume consists of an external mixture of cloud droplets and smoke aerosol particles. A cloud could be formed due to the lifting of hot humid air produced by fires. Radke et al. (1991) observed capping cumulus clouds over prescribed fires, which appears to be unlikely for the cases studied here though. Nevertheless, attempts were made where the smoke
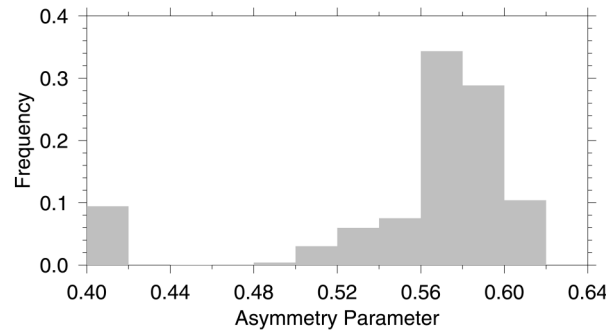
3. Summary

Aerosol optical depth is the most important quantity dictating aerosol radiative forcing. Smoke is a leading aerosol agent across the large North American boreal forest zone. In an attempt to retrieve smoke aerosol optical depth, it was found that heavy smoke plumes generated by boreal forest fires in Canada cannot be modeled using representative optical properties of biomass burning aerosols determined using data from previous field experiments such as SCAR-B, TRACE-A, BASE-A, ABLE-2A, and BOREAS. A successful retrieval would require a smoke aerosol model that produces significantly higher TOA reflectances than what the existing models predict. This can be achieved by a combination of an increase in the single scattering albedo and/or a decrease in the asymmetry parameter. Various factors affecting the two variables are explored based on observations from many sources, but few combinations can bring observations and model results into agreement. One possibility is that the smoke particles generated in Canadian boreal forest fires have lower ratios of black carbon to total carbon mass than the tropical fires. Some factors have offsetting effects in terms of single scattering albedo and asymmetry parameter such as the mean size of aerosol particles. For example, aerosols with small size distributions have low values of g (which increases TOA albedo) and ω (which decreases TOA albedo). A plausible explanation appears

to be the effect of relative humidity on smoke aerosol. Such an effect has not been studied thoroughly, especially in heavy smoke plumes. Since the humidity inside fresh heavy smoke plumes is expected to be much higher than in older disperse smoke, hygroscopic effects may be large enough to explain the discrepancy. This hypothesis seems to corroborate with the correlation between ω and τ and between g and τ derived from independent datasets. Even though the data are limited to relatively low optical depths, there are discernible trends that ω increases with τ, and g decreases with τ. Both trends help the retrieval of τ attempted in this work. Using these empirical relationships, the retrieval is feasible and the results are more plausible than those using the conventional values. We cannot, however, assess their absolute accuracy, since ground-based measurements of heavy smoke aerosols observed at or near fire locations are lacking. Another possibility that was considered is that the smoke plume is a mixture of smoke aerosols and cloud droplets. Water vapor, released by the burnt vegetation, is lifted with the hot air produced by the fire. This leads to cloud formation. It is possible to account for the high TOA reflectances observed with a smoke–cloud mixture, however, without further information the mixture cannot be modeled accurately. The hypotheses put forth in this paper are subject to substantiation from future field campaigns. Without this independent validation, this study can only suggest possible solutions to the problem—not the final solution.

REFERENCES

Anderson, B. E., and Coauthors, 1996: Aerosols from biomass burning over the tropical South Atlantic region: Distributions and impacts. *J. Geophys. Res.,* **101,** 24 117–24 137.

Andreae, M. O., and Coauthors, 1988: Biomass-burning emissions and associated haze layers over Amazonia. *J. Geophys. Res.,* **93,** 1509–1527.

Berk, A., L. S. Bernstein, and D. C. Robertson, 1989: MODTRAN: A moderate resolution model for LOWTRAN 7. Air Force Geophysics Laboratory Tech. Rep. GL-TR-89-0122.

Brest, C. L., W. B. Rossow, and M. D. Roiter, 1997: Update of radiance calibrations for ISCCP. *J. Atmos. Oceanic Technol.,* **14,** 1091–1109.

Chylek, P., and J. Wong, 1995: Effect of absorbing aerosols on global radiation budget. *Geophys. Res. Lett.,* **22,** 929–931.

——, and J. G. D. Wong, 1998: Erroneous use of the modified Kohler equation in cloud and aerosol physics applications. *J. Atmos. Sci.,* **55,** 1473–1477.

——, G. Videen, D. J. W. Geldart, J. S. Dobbie, and H. C. W. Tso, 2000: Effective medium approximations for heterogeneous particles. *Light Scattering by Nonspherical Particles: Theory, Measurements, and Applications,* M. I. Mishchenko et al., Eds., Academic Press, 273–308.

Cihlar, J., J. Chen, and Z. Li, 1997a: Seasonal AVHRR multichannel data sets and products for studies of surface–atmosphere interactions. *J. Geophys. Res.,* **102,** 29 625–29 640.

——, H. Ly, Z. Li, J. Chen, H. Pokrant, and F. Huang, 1997b: Multitemporal, multichannel AVHRR data sets for land biosphere studies—Artifacts and corrections. *Remote Sens. Environ.,* **60,** 35–57.

d'Almeida, G. A., P. Koepke, and E. P. Shettle, 1991: *Atmospheric Aerosols: Global Climatology and Radiative Characteristics,* A. Deepak Publishing, 561 pp.

Dubovik, O., B. N. Holben, Y. J. Kaufman, M. Yamasoe, A. Smirnov, D. Tanre, and I. Slutsker, 1998: Single-scattering albedo of smoke retrieved from the sky radiance and solar transmittance measured from ground. *J. Geophys. Res.,* **103,** 31 903–31 923.

Ferrare, R. A., R. S. Fraser, and Y. J. Kaufman, 1990: Satellite measurements of large-scale air pollution: Measurements of forest fire smoke. *J. Geophys. Res.,* **95,** 9911–9925.

Fishman, J., J. M. Hoell Jr., R. D. Bendura, R. J. McNeal, and V. W. J. H. Kirchhoff, 1996: NASA GTE TRACE A Experiment (September–October 1992): Overview. *J. Geophys. Res.,* **101,** 23 865–23 879.

Hale, G., and M. Querry, 1973: Optical constants of water in the 200 nm to 200 μm wavelength region. *Appl. Opt.,* **12,** 555–563.

Harriss, R. C., and Coauthors, 1988: The Amazon Boundary Layer Experiment (ABLE 2A): Dry season 1985. *J. Geophys. Res.,* **93,** 1351–1360.

Higurashi, A., and T. Nakajima, 1999: Development of a two-channel aerosol retrieval algorithm on a global scale using NOAA AVHRR. *J. Atmos. Sci.,* **56,** 924–941.

Hobbs, P. V., and Coauthors, 1996: Particle and trace-gas measurements in the smoke from prescribed burns of forest products in the Pacific Northwest. *Biomass Burning and Global Change: Biomass Burning in South America, Southeast Asia, and Temperate and Boreal Ecosystems, and the Oil Fires of Kuwait,* Vol. 2, J. S. Levine, Ed., MIT Press, 697–715.

——, ——, R. A. Kotchenruther, R. J. Ferek, and R. Weiss, 1997: Direct radiative forcing by smoke from biomass burning. *Science,* **275,** 1776–1778.

Holben, B. N., E. Vermote, Y. J. Kaufman, D. Tanre, and V. Kalb, 1992: Aerosol retrieval over land from AVHRR data—Application for atmospheric correction. *IEEE Trans. Geosci. Remote Sens.,* **30,** 212–222.

——, T. F. Eck, A. Setzer, I. Slutsker, A. Pereira, B. Markham, and J. V. Castle, 1996: Temporal and spatial variability of aerosol loading and properties during the Amazon, North American temperate, and boreal forest burning seasons. *Biomass Burning and Global Change: Biomass Burning in South America, Southeast Asia, and Temperate and Boreal Ecosystems, and the Oil Fires of Kuwait,* Vol. 2, J. S. Levine, Ed., MIT Press, 618–636.

——, and Coauthors, 1998: AERONET—A federated instrument network and data archive for aerosol characterization. *Remote Sens. Environ.,* **66,** 1–16.

Kaufman, Y. J., R. S. Fraser, and R. A. Ferrare, 1990: Satellite measurements of large-scale air pollution: Methods. *J. Geophys. Res.,* **95,** 9895–9909.

——, A. Setzer, D. Ward, D. Tanre, B. N. Holben, P. Menzel, M. C. Pereira, and R. Rasmussen, 1992: Biomass burning airborne and spaceborne experiment in the Amazonas (BASE-A). *J. Geophys. Res.,* **97,** 14 581–14 599.

——, B. N. Holben, D. Tanre, and D. E. Ward, 1994: Remote sensing of biomass burning in the Amazon. *Remote Sens. Rev.,* **10,** 51–90.

——, and Coauthors, 1997: Passive remote sensing of tropospheric aerosol and atmospheric correction for the aerosol effect. *J. Geophys. Res.,* **102,** 16 815–16 830.

——, and Coauthors, 1998: Smoke, Clouds, and Radiation–Brazil (SCAR-B) experiment. *J. Geophys. Res.,* **103,** 31 783–31 808.

Kidwell, K. B., 1991: NOAA polar orbiter data users guide. NOAA National Climate Data Center, Satellite Data Services Division.

King, M. D., Y. J. Kaufman, D. Tanre, and T. Nakajima, 1999: Remote

sensing of tropospheric aerosols from space: Past, present, and future. *Bull. Amer. Meteor. Soc.,* **80,** 2229–2259.

Konopka, P., 1996: A reexamination of the derivation of the equilibrium supersaturation curve for soluble particles. *J. Atmos. Sci.,* **53,** 3157–3163.

Kotchenruther, R. A., and P. V. Hobbs, 1998: Humidification factors of aerosols from biomass burning in Brazil. *J. Geophys. Res.,* **103,** 32 081–32 089.

Kou, L., D. Labrie, and P. Chylek, 1993: Refractive indices of water and ice in the 0.65- to 2.5-μm spectral range. *Appl. Opt.,* **32,** 3531–3540.

Li, Z., and L. Kou, 1998: The direct radiative effect of smoke aerosols on atmospheric absorption of visible sunlight. *Tellus,* **50B,** 543–554.

——, J. Cihlar, X. Zheng, L. Moreau, and H. Ly, 1996: The bidirectional effects of AVHRR measurements over boreal regions. *IEEE Trans. Geosci. Remote Sens.,* **34,** 1308–1322.

——, S. Nadon, and J. Cihlar, 2000: Satellite detection of Canadian boreal forest fires: Development and application of an algorithm, *Int. J. Remote Sens.,* **21,** 3057–3069.

——, A. Khananian, and R. Fraser, 2001: Detecting smoke from boreal forest fires using neural network and threshold approaches applied to AVHRR imagery. *IEEE Trans. Geosci. Remote Sens.,* **39,** 1859–1870.

Liousse, C., F. Dulac, H. Cachier, and D. Tanre, 1997: Remote sensing of carbonaceous aerosol production by African savanna biomass burning. *J. Geophys. Res.,* **102,** 5895–5911.

Markham, B. L., J. S. Schafer, B. N. Holben, and R. N. Halthore, 1997: Atmospheric aerosol and water vapor characteristics over north central Canada during BOREAS. *J. Geophys. Res.,* **102,** 29 737–29 745.

Martins, J. V., P. Artaxo, P. V. Hobbs, C. Liousse, H. Cachier, Y. Kaufman, and A. Plana-Fattori, 1996: Particle size distributions, elemental compositions, carbon measurements, and optical properties of smoke from biomass burning in the Pacific Northwest of the United States. *Biomass Burning and Global Change: Biomass Burning in South America, Southeast Asia, and Temperate and Boreal Ecosystems, and the Oil Fires of Kuwait,* Vol. 2, J. S. Levine, Ed., MIT Press, 716–732.

Mazurek, M. A., W. R. Cofer III, and J. S. Levine, 1991: Carbonaceous aerosols from prescribed burning of a boreal forest ecosystem. *Global Biomass Burning: Atmospheric, Climatic, and Biospheric Implications,* J. S. Levine, Ed., MIT Press, 258–263.

Miller, J. R., and N. T. O'Neill, 1997: Multialtitude airborne observations of insolation effects of forest fire smoke aerosols at BOREAS: Estimates of aerosol optical parameters. *J. Geophys. Res.,* **102,** 29 729–29 736.

Mishchenko, M. I., I. V. Geogdzhayev, B. Cairns, W. B. Rossow, and A. A. Lacis, 1999: Aerosol retrievals over the ocean by use of channels 1 and 2 AVHRR data: Sensitivity analysis and preliminary results. *Appl. Opt.,* **38,** 7325–7341.

Molineaux, B., A. Royer, and N. O'Neill, 1998: Retrieval of Pinatubo

aerosol optical depth and surface bidirectional reflectance from six years of AVHRR global vegetation index data over boreal forests. *J. Geophys. Res.,* **103,** 1847–1856.

Radke, L. F., and Coauthors, 1991: Particulate and trace gas emissions from large biomass fires in North America. *Global Biomass Burning: Atmospheric, Climatic, and Biospheric Implications,* J. S. Levine, Ed., MIT Press, 209–224.

Rao, C. R. N., and J. Chen, 1996: Post-launch calibration of the visible and near-infrared channels of the Advanced Very High Resolution Radiometer on the *NOAA-14* spacecraft. *Int. J. Remote Sens.,* **17,** 2743–2747.

Remer, L. A., Y. J. Kaufman, B. N. Holben, A. M. Thompson, and D. McNamara, 1998: Biomass burning aerosol size distribution and modeled optical properties. *J. Geophys. Res.,* **103,** 31 879–31 891.

Ross, J. L., P. V. Hobbs, and B. Holben, 1998: Radiative characteristics of regional hazes dominated by smoke from biomass burning in Brazil: Closure tests and direct radiative forcing. *J. Geophys. Res.,* **103,** 31 925–31 941.

Rossow, W. B., and R. A. Schiffer, 1999: Advances in understanding clouds from ISCCP. *Bull. Amer. Meteor. Soc.,* **80,** 2261–2287.

Schimel, D., and Coauthors, 1996: Radiative forcing of climate change. *Climate Change 1995: The Science of Climate Change,* J. T. Houghton et al., Eds., Cambridge University Press, 65–131.

Sellers, P. J., and Coauthors, 1997: BOREAS in 1997: Experimental overview, scientific results, and future directions. *J. Geophys. Res.,* **102,** 28 731–28 769.

Soufflet, V., D. Tanre, A. Royer, and N. T. O'Neill, 1997: Remote sensing of aerosols over boreal forest and lake water from AVHRR data. *Remote Sens. Environ.,* **60,** 22–34.

Stamnes, K., S.-C. Tsay, W. Wiscombe, and K. Jayaweera, 1988: Numerically stable algorithm for discrete-ordinate-method radiative transfer in multiple scattering and emitting layered media. *Appl. Opt.,* **27,** 2502–2509.

Stocks, B. J., 1991: The extent and impact of forest fires in northern circumpolar countries. *Global Biomass Burning: Atmospheric, Climatic, and Biospheric Implications,* J. S. Levine, Ed., MIT Press, 197–202.

Stowe, L. L., A. M. Ignatov, and R. R. Singh, 1997: Development, validation, and potential enhancements to the second-generation operational aerosol product at the National Environment Satellite, Data, and Information Service of the National Oceanic and Atmospheric Administration. *J. Geophys. Res.,* **102,** 16 923–16 934.

Toon, O. B., and T. P. Ackerman, 1981: Algorithms for the calculation of scattering by stratified spheres. *Appl. Opt.,* **20,** 3657–3660.

WMO, 1986: A preliminary cloudless standard atmosphere for radiation computation. World Meteorological Organization Tech. Rep. WCP-112, 53 pp.

Yamasoe, M. A., Y. J. Kaufman, O. Dubovik, L. A. Remer, B. N. Holben, and P. Artaxo, 1998: Retrieval of the real part of the refractive index of smoke particles from sun–sky measurements during SCAR-B. *J. Geophys. Res.,* **103,** 31 893–31 902.